Boundary Conditions for Collisional Granular Flows of Frictional and Rotational Particles at Flat Walls

Yunhua Zhao and Yingjie Zhong
College of Mechanical Engineering, Zhejiang University of Technology, Hangzhou 310014, China

Yurong He
School of Energy Science and Engineering, Harbin Institute of Technology, Harbin 150001, China

H. Inaki Schlaberg
School of Control and Computer Engineering, North China Electric Power University, Beijing 102206, China

DOI 10.1002/aic.14596
Published online August 25, 2014 in Wiley Online Library (wileyonlinelibrary.com)

Collisions between frictional particles and flat walls are determined using Coulomb friction and both tangential and normal restitution, and pseudothermal states of particles are described by both the translational and rotational granular temperatures. Then, new models for the stresses and the fluxes of fluctuation energy for the collisional granular flows at the walls are derived. These new models are tested and compared with the literature data and models. The ratio of rotational to translational granular temperatures is shown to be crucial on accurately predicting the shear stress and energy flux and is dependent on the normalized slip velocity as well as the collisional parameters. Using a theoretical but constant value for this ratio, predictions by the new models could still agree better with the literature data than those by the previous models. Finally, boundary conditions are developed to be used within the framework of kinetic theory of granular flow. © 2014 American Institute of Chemical Engineers *AIChE J*, 60: 4065–4075, 2014
Keywords: boundary condition, particle rotation, frictional collision, kinetic theory of granular flow, two-fluid model

Introduction

Gas–solid multiphase flows are involved in numerous industrial applications, such as energy production, metallurgical, pharmaceutical, food and agricultural processing. To simulate the gas–solid flows in those various systems, the Euler–Euler two-fluid model has emerged as a very promising tool due to its compromise between computational cost, level of detail provided, and potential of applicability.[1,2]

In the two-fluid model, both the gas and solid phases are treated as fully interpenetrating continua, and are described by separate conservation equations for mass and momentum. Owing to the continuum representation of the particulate suspension, additional closures are required for the solid-phase constitutive relations. The kinetic theory of granular flow (KTGF), basically an extension of the classical kinetic theory of dense gas molecules to granular particles, is extensively used to derive the solid-phase constitutive relations.[3,4] In the original KTGF, solid particles are assumed to be inelastic smooth spheres. Thus, only normal impact and rebound velocities of two colliding particles are related using the coefficient of normal restitution, while the tangential velocities and spins remain the same. As a consequence, the pseudothermal state of the particles can be described by merely the translational granular temperature, which characterizes the intensity of the translational velocity fluctuations.

In realistic systems, particles are always frictional as well as inelastic. So far, great efforts have been made to incorporate the effect of particle friction into the KTGF.[5–13] To describe the frictional particle collisions, the combination of the Coulomb friction coefficient and both tangential and normal restitution coefficients is suggested.[9,13] Then, the particle spins can be changed through contact friction or tangential inelasticity, so the pseudothermal state of the particles needs to be described by both the translational and rotational granular temperatures, and the latter one is to characterize the intensity of rotational velocity fluctuations. By solving the rotational granular temperature in an explicit way, Jenkins and Zhang[9] derived an effective coefficient of restitution for the original KTGF. In recent years, this effective coefficient approach has been successfully applied to simulate dense gas–solid flows.[14–19]

In addition to the KTGF, the wall boundary conditions (BCs) induced by particle-wall collisions are reported to play important roles in numerically simulating various gas–solid flows.[20–25] Unlike gas flow, granular particle flow commonly experiences a significant relative average velocity between the flow particles and the boundary wall. Furthermore, the wall may supply fluctuation energy to the particle flow from the working of its shear stress through the relative velocity. Therefore, BCs for the particle flows must be calculated, rather than assumed.[26]

Generally, there are two main approaches for incorporating the physics of particle-wall collisions into the kinetic theory

Correspondence concerning this article should be addressed to Y. Zhao at zhaoyh@zjut.edu.cn.

models. Johnson and Jackson[27] proposed BCs in a heuristic way by assuming some particles collide and the rest slide relative to the boundary. The particle sliding refers to enduring contact and results in frictional contributions to the momentum and energy transfer, while the particle colliding is instantaneous and results in collisional contributions. For rapid granular flows, the frictional contributions are always neglected, as the collisional contributions are dominant. The colliding particle is characterized by the normal restitution coefficient and a specularity coefficient, which can range from 0 to 1, with a zero value for perfectly specular collisions and a value of unity for completely diffuse collisions. Physically, Johnson and Jackson BCs do not distinguish between sticking and sliding collision, and the value of specularity coefficient depends on the flow state, wall roughness, and particle-wall friction. This causes great difficulties in measurement, so that no experimental value of the specularity coefficient has been reported in the open literature to the best of our knowledge. However, the Johnson and Jackson BCs are widely used due to their relative simplicity and validity, if the specularity coefficient is properly set.[22,24,25] Conversely, Jenkins[28] proposed flat wall BCs using Coulomb friction and both tangential and normal restitution, which are actually measurable properties. In Jenkins BCs, frictional particle-wall collisions could be either sticking or sliding, thus the collisional exchanges of momentum and fluctuation energy are analytically expressed in two asymptotic circumstances, namely the nonsliding limit and the all-sliding limit. Jenkins and Louge[29] later refined the calculation of flux of fluctuation energy at the wall, and additionally extended the expression for the nonsliding limit to incorporate small sliding. Benyahia et al.[20] applied the Jenkins and Louge BCs in modeling the dilute turbulent gas–solid flow in a pipe, and found that the experimental data fell between the nonsliding and all-sliding limits, whereas the physical behavior of the particle-wall interactions was close to the all sliding limit. This implies that general expressions of BCs which cover all possible circumstances between the two limits are required. Recently, Schneiderbauer et al.[30] derived new BCs connecting sticking and sliding collisions in one expression, and including compressible effects of the particle flow. They also demonstrated that their BCs could significantly improve the agreement between the numerical predictions and the experimental measurements of dense gas–solid flows in a spouted bed.[31] However, these BCs only take account of the particle translational granular temperature, but ignore the rotational granular temperature, which may have some impact on the exchange of momentum and fluctuation energy at the wall.

The objective of this study is to propose wall BCs, which must meet the following two requirements. First, the BCs are consistent with Jenkins and Zhang's theory[9] on a fundamental basis. This means a collision model with three coefficients and a pseudothermal state with two granular temperatures are adopted, so that the resulting BCs can be reasonably used along with the effective coefficient approach. Second, the BCs are expressed in more general forms, which could cover the whole range from the nonsliding to the all-sliding limits.

Theoretical Methods

Particle-wall collision

Following Jenkins,[28] analysis of particle-wall collisions in this study are based on the following assumptions: (1) the particles are identical and homogeneous rigid spheres; (2) the wall is a flat and impermeable rigid body; (3) collisions are instantaneous with a point contact, interaction forces are impulsive and all other finite forces are negligible during collisions. As shown in Figure 1, the particle has translational velocity $\mathbf{c}$ and rotational velocity $\boldsymbol{\omega}$ before a collision; the corresponding postcollision velocities are primed. Then, the velocities before and after a collision are related by

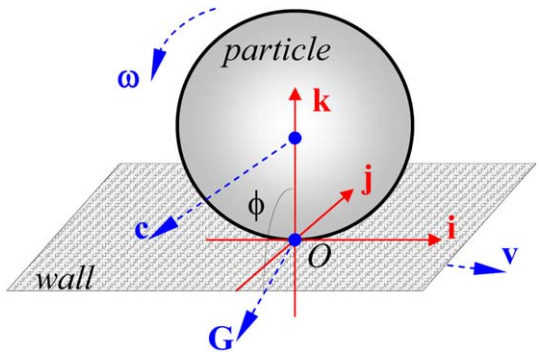

Figure 1. Schematic illustration of particle-wall collision.

[Color figure can be viewed in the online issue, which is available at wileyonlinelibrary.com.]

$$m(\mathbf{c}'-\mathbf{c})=\mathbf{J} \tag{1}$$

$$I(\omega'-\boldsymbol{\omega})=\frac{\sigma}{2}\mathbf{J}\times\mathbf{k} \tag{2}$$

where m is the mass, σ is the diameter, and $I=m\sigma^2/10$ is the moment of rotary inertia about the center of the sphere. $\mathbf{J}$ denotes the impulse supplied by the wall, and the unit vector $\mathbf{k}$ is normal to the wall and pointing into the flow. To completely determine the impulse, the relative velocity of the point of contact is introduced by

$$\mathbf{G}=\mathbf{c}-\frac{\sigma}{2}\boldsymbol{\omega}\times\mathbf{k}-\mathbf{v} \tag{3}$$

where $\mathbf{v}$ is the velocity of the moving wall.

In a sliding collision, the impulse can be written as

$$\mathbf{J}^{(\mathrm{sl})}=-m(1+e)(\mathbf{G}\cdot\mathbf{k})\mathbf{k}-m\mu(1+e)\cot\phi(\mathbf{G}\times\mathbf{k})\times\mathbf{k} \tag{4}$$

where e is the normal restitution coefficient, μ is the coefficient of Coulomb friction, and ϕ is the collision angle between $\mathbf{G}$ and $\mathbf{k}$. To ensure the collisions happen, ϕ must be located between $\pi/2$ and π. As ϕ increases, the sliding could stop and a sticking collision occurs. The impulse in a sticking collision can be obtained as

$$\mathbf{J}^{(\mathrm{st})}=-m(1+e)(\mathbf{G}\cdot\mathbf{k})\mathbf{k}+m\frac{q}{1+q}(1+\beta_0)(\mathbf{G}\times\mathbf{k})\times\mathbf{k} \tag{5}$$

where β_0 is the tangential restitution coefficient and $q=4I/m\sigma^2$ is the dimensionless moment of inertia.

When Eqs. 4 and 5 are equal to each other, a critical value Φ for the collision angle is determined such that

$$\cot\Phi=-\frac{q}{1+q}\frac{(1+\beta_0)}{(1+e)\mu} \tag{6}$$

Note that for $\phi\le\Phi$ the sliding collisions happen, otherwise sticking collisions occur. In practice, the three collisional parameters, e, β_0, and μ, are physically measurable

and could give a reasonably accurate description of experiments performed with real particles.[32–35] Strictly speaking, the normal restitution coefficient always decreases with the increase of impact velocity,[32,36] and the tangential restitution coefficient is also affected by the impact angle.[37,38] However, it is usually safe to assume these coefficients to be constant,[39] so this assumption is used in the following analysis.

Collisional rate of change

For a given particle property ψ that is a function of $\mathbf{c}$ and $\boldsymbol{\omega}$, its local and instantaneous average is defined using a particle velocity distribution function $f(\mathbf{c}, \boldsymbol{\omega})$ as

$$\langle\psi\rangle = \frac{1}{n}\int\int \psi(\mathbf{c},\boldsymbol{\omega}) f(\mathbf{c},\boldsymbol{\omega}) d\mathbf{c} d\boldsymbol{\omega} \tag{7}$$

where n is the number density of particles. Then, the mean translational velocity $\mathbf{u}$ is $\langle\mathbf{c}\rangle$, and the mean rotational velocity $\boldsymbol{\varpi}$ is $\langle\boldsymbol{\omega}\rangle$. The corresponding fluctuating velocities are denoted by $\mathbf{C} = \mathbf{c} - \mathbf{u}$ and $\boldsymbol{\Omega} = \boldsymbol{\omega} - \boldsymbol{\varpi}$. The translational granular temperature is defined by $T = \langle\mathbf{C}\cdot\mathbf{C}\rangle/3$, and the rotational granular temperature by $\Theta = I\langle\boldsymbol{\Omega}\cdot\boldsymbol{\Omega}\rangle/3m$.[9] In an average sense, the relative velocity of the granular flow to the boundary wall is $\mathbf{V} = \langle\mathbf{G}\rangle$. For the impermeable wall, $\mathbf{V}\cdot\mathbf{k}$ equals zero, thus $\mathbf{V}$ is actually the slip velocity and parallel to the wall.

In a collision with the wall, the particle property changes from ψ to ψ', which can be determined according to Eqs. 1, 2, and 4 or 5. Then, the collisional rate of change per unit area of the wall, Coll(ψ), is the integral of the change in ψ in a single collision over all possible collisions[28]

$$\mathrm{Coll}(\psi) = -\chi\int\int_{\mathbf{G}\cdot\mathbf{k}<0} (\psi'-\psi) f(\mathbf{c},\boldsymbol{\omega})(\mathbf{G}\cdot\mathbf{k}) d\mathbf{c} d\boldsymbol{\omega} \tag{8}$$

where χ is a factor that takes into account the presence of the wall on the spatial distribution of the particles.

To enable the calculation of Coll(ψ), knowledge of the particle velocity distribution in the near wall region is required. Jenkins[28] ignored the fluctuations in rotational velocity and proposed a delta function for the distribution of translational velocity fluctuations. Later, computer simulations by Louge[26] revealed that the normal component of the translational velocity fluctuation was completely different to the delta distribution, and the tangential components complied to a Maxwellian distribution. Jenkins and Louge[29] used an isotropic Maxwellian distribution for all the tangential and normal components of the translational velocity fluctuation, they also estimated the error introduced using the Maxwellian distribution was no greater than 30%. Hence, using the Maxwellian distribution for the fluctuations of translational velocity is preferred in recent studies of the BCs.[30,39] When both the translational and rotational velocities were concerned, McCoy et al.[40] proposed a two-temperature Maxwellian distribution. So far, this simple distribution function has been commonly adopted to study granular flows in the literature.[8,9,11] It should be noted that the Maxwellian distribution is established from the steady state, and the actual distribution may have perturbations due to the spatial gradients of the mean fields.[9] However, those perturbations have seldom been considered in the study of BCs. One of the main reasons may be that they lead to complex integrations but the accuracy remains uncertain. At this point, we apply the two-temperature Maxwellian distribution as follows[9,40]

$$f(\mathbf{c},\boldsymbol{\omega}) = n\left(\frac{1}{2\pi T}\right)^{\frac{3}{2}}\left(\frac{I}{2\pi m\Theta}\right)^{\frac{3}{2}}\exp\left(-\frac{\mathbf{C}\cdot\mathbf{C}}{2T} - \frac{I\boldsymbol{\Omega}\cdot\boldsymbol{\Omega}}{2m\Theta}\right) \tag{9}$$

Using Eq. 8 with $\psi = mC_k$, the collisional rate of change is the normal stress applied by the wall to the granular flow. As the integration is straightforward, upon carrying it out yields

$$N = \mathrm{Coll}(mC_k) = mn\chi(1+e)\frac{T}{2} \tag{10}$$

Similarly, letting ψ be the tangential momentum, mC_i, the collisional rate of change turns out to be the shear stress along the i direction. Unfortunately, we are only able to derive an analytical expression as

$$\begin{aligned} S_i = \mathrm{Coll}(mC_i) = mn\chi\frac{\mu(1+e)}{4\pi(\lambda+1)}\int\frac{G_i}{G_{ij}} \\ \times\mathrm{erf}\left(\frac{G_{ij}\cot\Phi}{\sqrt{2T}}\right)\exp\left[\frac{-|\mathbf{G}_{ij}-\mathbf{V}|^2}{2T(\lambda+1)}\right] d\mathbf{G}_{ij} \end{aligned} \tag{11}$$

where $\lambda = \Theta/(qT)$ is a particular ratio of the rotational to translational granular temperatures, and $\mathbf{G}_{ij}$ is the component of $\mathbf{G}$ in the i-j plane (see Figure 1). As shown in Appendix A, approximated expressions for S_i can be obtained. In a normalized form, the shear stress is written as

$$\frac{S_i}{N} = \mu\cot\Phi\sqrt{\frac{2}{\pi T}}V_i\max(A_1, B_1) \tag{12}$$

where

$$\begin{aligned} A_1 = \frac{1}{2}\left(\frac{1}{X^2+1} + \frac{\arctan X}{X}\right) \\ -\frac{Y^2}{8X^2}\left[\frac{X^2-1}{(X^2+1)^2} + \frac{\arctan X}{X}\right], \quad X = \sqrt{\lambda+1}\cot\Phi \end{aligned} \tag{13}$$

$$\begin{aligned} B_1 = \frac{\sqrt{\pi}}{2}\frac{\mathrm{erf}(Y)}{Y} - \frac{X^2}{4Y^2} \\ \times\left[\frac{\sqrt{\pi}}{2}\frac{\mathrm{erf}(Y)}{Y} + (2Y^2-1)\exp(-Y^2)\right], \quad Y = \sqrt{\frac{V^2}{2T}}\cot\Phi \end{aligned} \tag{14}$$

It can be found that S_i and V_i are opposite in their directions, and this means the shear stress is always generated to stop the slip. It should also be mentioned that the expression for shear stress contains two competing components, which are indeed approaching the nonsliding and all-sliding limits, respectively. However, it is not an interpolation between the two limits, but just a numerical approximation of Eq. 11. Thus, we think it is still in a general form that can cover all circumstances.

Considering Eq. 8 with $\psi = m(\mathbf{C}\cdot\mathbf{C})/2$, the flux of translational fluctuation energy that is supplied by the wall to the flow is obtained as

$$\begin{aligned} Q_t &= \mathrm{Coll}\left(\frac{m}{2}\mathbf{C}\cdot\mathbf{C}\right) \\ &= mn\chi T\sqrt{\frac{T}{2\pi}}\left\{-(1-e^2)+\mu^2(1+e)^2\left[1-\frac{1}{X^2+1}\exp\left(-\frac{Y^2}{X^2+1}\right)\right]\right\} \\ &+ mn\chi\frac{\mu(1+e)}{4\pi(\lambda+1)^2}\int\frac{\mathbf{G}_{ij}\cdot(\mathbf{G}_{ij}-\mathbf{V})}{G_{ij}}\mathrm{erf}\left(\frac{G_{ij}\cot\Phi}{\sqrt{2T}}\right)\exp\left[\frac{-|\mathbf{G}_{ij}-\mathbf{V}|^2}{2T(\lambda+1)}\right] d\mathbf{G}_{ij} \end{aligned} \tag{15}$$

Again, as shown in Appendix B, an approximate expression is given by

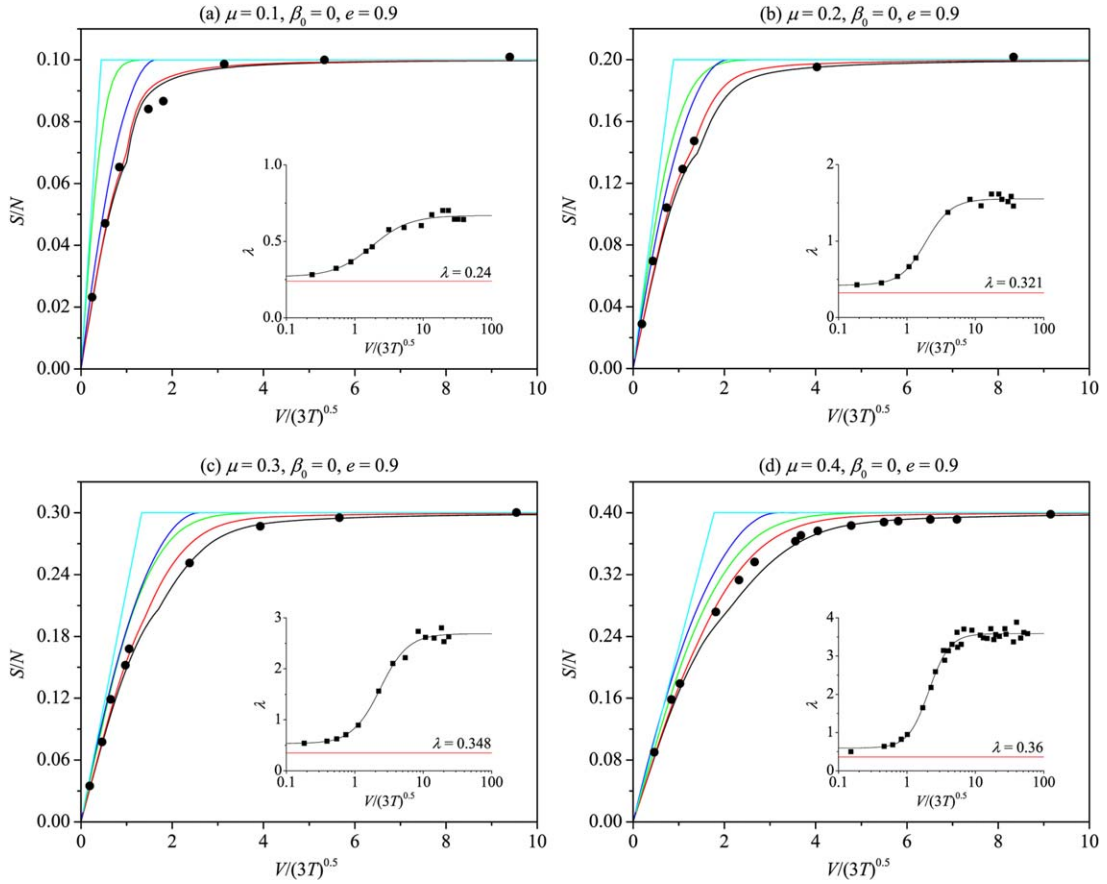

Figure 2. Stress ratio over normalized slip velocity for different coefficients of friction.

(Circle •: Louge's data; black line ——: present model with fitted λ; red line ——: present model with constant λ; green line ——: Schneiderbauer et al.'s model; blue line ——: Li et al.'s model; Cyan line ——: Jenkins' model. Inset: granular temperature ratio, λ, over normalized slip velocity, with square ■: Louge's data; black line ——: Logistic fit; red line ——: Jenkins and Zhang's theory.) [Color figure can be viewed in the online issue, which is available at wileyonlinelibrary.com.]

$$\frac{Q_t}{N\sqrt{3T}} = \sqrt{\frac{2}{3\pi}}\left\{\mu^2(1+e)\left[1-\frac{1}{X^2+1}\exp\left(-\frac{Y^2}{X^2+1}\right)\right] - (1-e) + \mu\cot\Phi\min(A_2, B_2)\right\} \tag{16}$$

where

$$A_2 = \frac{1}{X^2+1} + \frac{\arctan X}{X} - \frac{Y^2}{2X^2}\left[\frac{X^2-1}{(X^2+1)^2} + \frac{\arctan X}{X}\right] + \frac{3Y^4}{16X^4}\left[\frac{(3X^2+1)(X^2-3)}{3(X^2+1)^3} + \frac{\arctan X}{X}\right] \tag{17}$$

$$B_2 = \left(1+\frac{X^2}{16Y^2}\right)\frac{\sqrt{\pi}}{2}\frac{\mathrm{erf}(Y)}{Y} + \exp\left(-Y^2\right) \tag{18}$$

Similarly, if ψ being $I(\mathbf{\Omega}\cdot\mathbf{\Omega})/2$, the corresponding flux of rotational fluctuation energy is approximated as

$$\frac{Q_r}{N\sqrt{3T}} = \sqrt{\frac{2}{3\pi}} \left\{\frac{\mu^2(1+e)}{q}\left[1-\frac{1}{X^2+1}\exp\left(-\frac{Y^2}{X^2+1}\right) + \lambda\mu\cot\Phi\max(A_2, B_2)\right]\right\} \tag{19}$$

Results and Discussion

Comparison of wall stress

To test the above analyses, the ratio between the magnitudes of the normal and tangential components of the wall stress, S/N, is compared with previous theoretical studies[28,30,39] as well as the numerical results from particle simulations by Louge.[26] It should be noted that direct experimental data are not available at present for quantitative verification.

Figure 2 shows the stress ratio over the normalized slip velocity, $V/(3T)^{0.5}$, for different values of μ. In the present model, the granular temperature ratio λ is required. Thus, as shown in the insets, λ is obtained by fitting the Louge's particle simulation data, or more practically through Jenkins and Zhang's theory as listed in Table 1. It is found that Logistic functions for λ can fit Louge's data very well, but according to Jenkins and Zhang's theory λ remain constants for the specified collisional parameters. The stress ratios predicted by the present models with both fitted and constant λ are plotted, respectively. It can be seen that the gap caused

Table 1. Granular Temperature Ratio Based on Jenkins and Zhang's Theory[9]

$\lambda = \dfrac{b_1}{qb_2}$
$b_1 = \left(\dfrac{\mu}{\mu_0}\right)^2 \dfrac{\mu_0^2}{1+\mu_0^2}$
$b_2 = \dfrac{1}{2}\dfrac{\mu}{\mu_0}\left[\dfrac{\pi}{2}\mu_0\left(1-\dfrac{2}{\pi}\arctan\mu_0\right) + \dfrac{\mu_0^2}{1+\mu_0^2}\right]$
$\mu_0 = \dfrac{7}{2}\dfrac{\mu(1+e)}{1+\beta_0}$

Table 2. Summary of Previous Models for the Stress Ratio

Li et al.[39]

$$\frac{S}{N}=\frac{\sqrt{6\pi}}{1+e}r\phi'$$

$$\text{where } \phi'=\begin{cases}\phi'_0-\dfrac{7\sqrt{6\pi}\left(\phi'_0\right)^2}{8k}r, & r\le\dfrac{4k}{7\sqrt{6\pi}\phi'_0}\\ \dfrac{2k}{7\sqrt{6\pi}r}, & \text{otherwise}\end{cases},\ k=\frac{7}{2}\mu(1+e),$$

$$\text{and } \phi'_0=-0.0012596+0.10064551k-0.04281476k^2+0.0097594k^3-0.0012508258k^4+0.0000836983k^5-0.00000226955k^6,\quad k\in(0,10)$$

Schneiderbauer et al.[30]

$$\frac{S}{N}=\mu\mathrm{erf}\left(\sqrt{\frac{3}{2}}\frac{r}{\mu_0}\right),\ \mu_0=\frac{7}{2}\frac{\mu(1+e)}{1+\beta_0}$$

Jenkins[28]

$$\frac{S}{N}=\frac{\mu}{\mu_0}R,\ R=\begin{cases}\dfrac{3}{2}r, & 1^{a}\le r\le\dfrac{2\mu_0}{3}\\ \mu_0, & \dfrac{2\mu_0}{3}\le r\le\infty\end{cases}$$

[a]The restriction on $r\ge 1$ is always neglected in practice.

by using fitted or constant λ is only obvious in the transition regime between the nonsliding and all-sliding limits. Furthermore, the larger μ is, the greater the gap is. For comparison, those stress ratios predicted from previous models (see Table 2) and the corresponding Louge's data are also plotted in Figure 1. In general, the present model with fitted λ seems to be the best one to resemble Louge's data, and followed by the present model with constant λ. Therefore, a combination of the present model and constant λ by Jenkins and Zhang's theory may give acceptable predictions of the stress ratio. Besides, it can be also found that the stress ratio for a given normalized slip velocity increases greatly with the increase of μ, and this trend can be obtained from all the theoretical models. In the all-sliding limit, the stress ratio is simply equal to μ, because the tangential impulse is limited by Coulomb friction in each sliding collision. In contrast, Johnson and Jackson BC predicts a linear dependence of the stress ratio on the normalized slip velocity if the frictional contribution to momentum transfer is neglected. Therefore, as pointed out by Schneiderbauer et al.,[30] the stress ratio at high slip velocity is overestimated by Johnson and Jackson BC, and it is common to use low values for specularity coefficient to model the physical limit of Coulomb friction.

Figure 3 shows the stress ratio over the normalized slip velocity for different values of β_0. As can be observed, stress ratios predicted by the present model with constant λ agree better with Louge's data than those by of the previous models. In the insets, the discrete values of λ are solved from Eq. 12 with Louge's data for S/N, because the corresponding λ values for these cases, except the one in subfigure (a), are not directly provided by Louge.[26] It is unsurprising that those discrete λ values would fit well using the Logistic functions, and

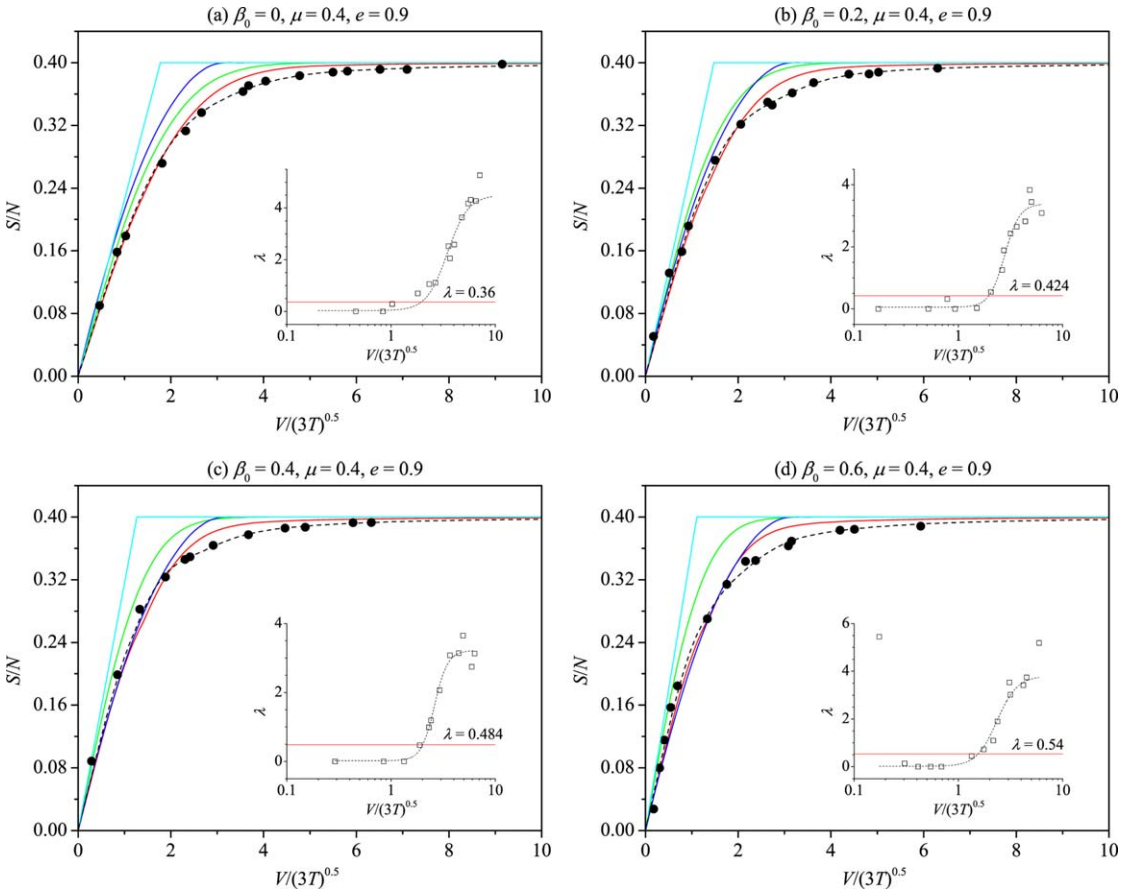

Figure 3. Stress ratio over normalized slip velocity for different coefficients of tangential restitution.

(Circle •: Louge's data; black dashed line – – –: present model with fitted λ; red line ——: present model with constant λ; green line ——: Schneiderbauer et al.'s model; blue line ——: Li et al.'s model; Cyan line ——: Jenkins' model. Inset: granular temperature ratio over normalized slip velocity, and open circle □: solved from Eq. 12 with Louge's data; black line ——: Logistic fit; red line ——: Jenkins and Zhang's theory.) [Color figure can be viewed in the online issue, which is available at wileyonlinelibrary.com.]

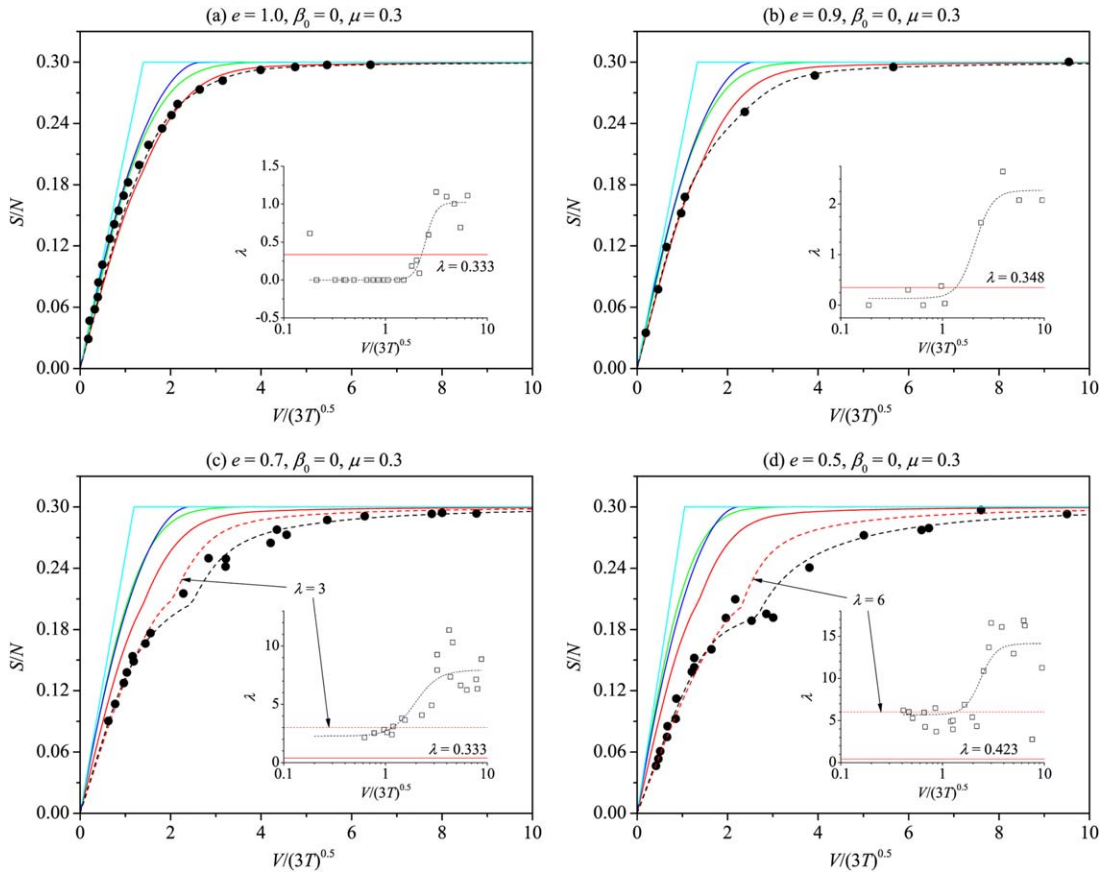

Figure 4. Stress ratio over normalized slip velocity for different coefficients of normal restitution.

(The lines and symbol have the same meaning as in Figure 3. Besides, red dashed line – – –: present model with specified λ. Inset: red dashed line – – –: specified λ.) [Color figure can be viewed in the online issue, which is available at wileyonlinelibrary.com.]

the present model with fitted λ values matches the *S/N* data fairly well. When the discrete λ values in the insets of Figures 3a and 2d are compared, they are qualitatively consistent with each other although having differences in quantity, and this could imply that the present model does correctly include some intrinsic connection between λ and *S/N*. Additionally, by increasing β_0, the stress ratio for normalized slip velocity in the small sliding regime increases slightly, that is, the profile is shifted toward the left. But this trend cannot be obtained from Li et al.'s model, as β_0 is not involved in there.

Figure 4 shows the stress ratio over the normalized slip velocity for different values of *e*. When compared with those previous models, the present model with constant λ based on Jenkins and Zhang's theory generally gets closer predictions to Louge's data, and furthermore its predictions are fairly good for nearly elastic particles (e.g., $e = 1$ or 0.9), but gets worse for highly inelastic particles (e.g., $e = 0.7$ or 0.5). As *e* decreases, the stress ratio profiles predicted by the previous models and the present model with the constant λ are shifted slightly leftward, whereas the distributions of Louge's data have a clear rightward shift. As for the reason, Schneiderbauer et al.[30] stated that the hypothesis of Maxwellian velocity distribution was not valid for highly inelastic particles near the wall, and the negligence of the tangential relative velocity distribution also contributed to the differences. Li et al.[39] indicated that there could be many reasons, including isotropic assumption on granular temperature, ignorance of particle rotation, as well as the use of Maxwellian velocity distribution. Interestingly, it is found that the great differences can be addressed in the present model by adjusting λ. As observed in the insets of Figures 4c, d, λ solved from Eq. 12 still obeys the Logistic functions with regard to the normalized slip velocity, but they are comparatively large even in the small sliding regime. Through increasing λ, $\lambda = 3$ and $\lambda = 6$ are intuitively specified for cases of $e = 0.7$ and $e = 0.5$, respectively, the results predicted with the present model significantly move toward the Louge's data. Thus, the present model can be used for a broad range of collisional parameters, as long as λ is well specified. In addition, it may also be concluded that particle inelasticity plays an important role on the fluctuation energy partition between rotational and translational modes. To get more realistic values for λ, one can solve conservation equations for both translational and rotational granular temperatures.[13] However, this may be still unsatisfied for situations of highly inelastic particles, because the previous kinetic theory models are commonly established by assuming the single particle velocity distribution function is a small perturbation from the local equilibrium distribution function.[3,7,9,13] In other words, these models are theoretically suitable for nearly elastic particles, and fundamental models for highly elastic particles are worth further research.

Comparison of energy flux

The total flux of fluctuation energy at the wall can be obtained by summing Eqs. 16 and 19. As shown in Figure 5a, the normalized flux is plotted over the normalized slip velocity under different values of μ. For the purpose of

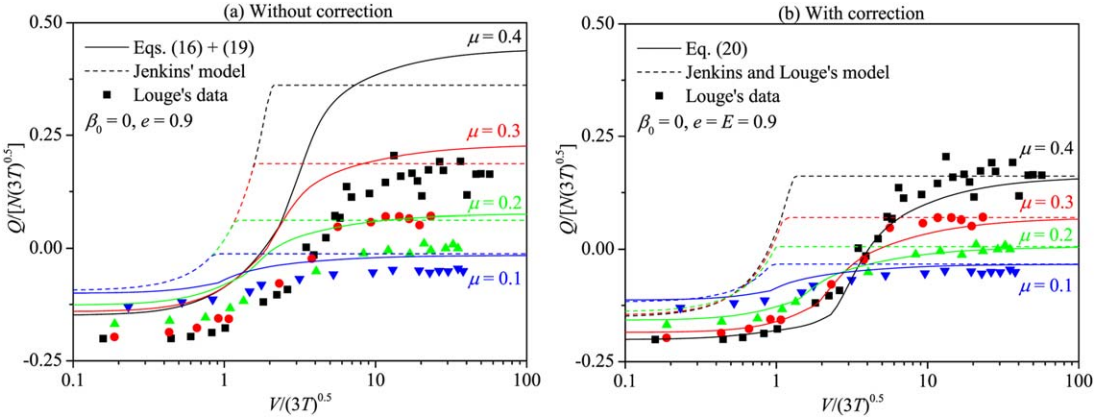

Figure 5. Effect of the correction on prediction of the fluctuation energy flux.

[Color figure can be viewed in the online issue, which is available at wileyonlinelibrary.com.]

comparison, the predictions with Jenkins' model as listed in Table 3 and the simulation results of Louge[26] are also plotted together. As observed, this new model quantitatively fails to fully resemble Louge's data, although it still shows better advantages than Jenkins's model, especially for cases of low friction (e.g., $\mu = 0.1$ or 0.2).

To refine the calculation of energy flux, additional assumptions were always made in the previous works, for example, Jenkins and Louge[29] introduced an approximation to the correlations between the normal and tangential components of the relative velocity, while Schneiderbauer et al.[30] applied approximations for the particle spin based on the Louge's data. In the all-sliding limit, the total flux of fluctuation energy calculated with Eqs. 16 and 19 reduces to

$$\frac{Q}{N\sqrt{3T}} = \sqrt{\frac{2}{3\pi}}\left[\frac{1+q}{q}\mu^2(1+e) - (1-e)\right] \tag{20}$$

Compare Eq. 20 with Jenkins and Louge's model (see Table 3), a correction factor can be easily obtained and the energy flux is then modified to be

$$\frac{Q}{N\sqrt{3T}} = \sqrt{\frac{2}{3\pi}}\left\{\frac{2-eE}{2+eE}\frac{1+q}{q}\mu^2(1+e) \times\left[1-\frac{1}{X^2+1}\exp\left(-\frac{Y^2}{X^2+1}\right)\right] - (1-e) + (1+\lambda)\mu\cot\Phi\min(A_2, B_2)\right\} \tag{21}$$

where E is the coefficient of normal restitution for particle–particle collisions. As indicated by Jenkins and Louge,[29] the use of E implies that the particle colliding to the wall may retain a "memory" (physically, the postcollisional properties) of earlier collision with interior particle. Actually, it can be found that the correction factor is exerted on the integral of the tangential fluctuation energy, and its value is smaller than unity. This can be explained by the anisotropic nature of particle fluctuation, which has been shown that the second-order moments of tangential velocity fluctuations are greatly confined in the near wall region.[26] In addition, this anisotropy is probably caused by the presence of the wall, so that the correction will not disappear even for ideal elastic particles. The corresponding normalized energy fluxes predicted with Eq. 21 and Jenkins and Louge's model are plotted in Figure 5b. As can be observed, owing to this correction, Eq. 21 seems quite accurate in the whole range of the normalized slip velocity.

It should be noted that the present models in Figure 5 are using fitted values of λ, which are obtained from the insets in Figure 2. However, it is more convenient to obtain a constant λ from the theory of Jenkins and Zhang.[9] As shown in Figure 6, combining Eq. 21 and Jenkins and Zhang's theory, the present model predicts the normalized fluctuation energy fluxes over the normalized slip velocity under different collisional parameters. For comparison, predictions with the most recent model by Schneiderbauer et al.[30] (see Table 3) and the corresponding Louge's data are plotted together. Figure 6a shows that the energy fluxes predicted by the present model can agree better to Louge's data than those by

Table 3. Summary of Previous Models for the Energy Flux

Jenkins[28]

$\frac{Q}{N\sqrt{3T}} = \frac{2(1+\beta_0)}{7(1+e)}FF - \frac{3}{8}(1-e)$

where

$$FF = \begin{cases} \frac{3}{8}\left[2(1+\beta_0)r^2 - (1-\beta_0)\right], & 1^{a} \le r^2 \le \frac{1}{2}\left(\mu_0^2 + \frac{1-\beta_0}{1+\beta_0}\right) \\ \frac{3}{8}(1+\beta_0)\mu_0^2, & \frac{1}{2}\left(\mu_0^2 + \frac{1-\beta_0}{1+\beta_0}\right) \le r^2 \le \infty \end{cases}$$

$r = \frac{V}{\sqrt{3T}}$, $\mu_0 = \frac{7}{2}\frac{\mu(1+e)}{1+\beta_0}$

Jenkins and Louge[29]

$$\frac{Q}{N\sqrt{3T}} = -\sqrt{\frac{\pi}{6}}\left\{\frac{2}{\pi}(1-e) + \frac{\mu}{\mu_0}\sin^4\phi_0\left[(1-\beta_0)(1-2r^2\cos 2\phi_0) - 4r^2\right] + \frac{\mu}{2}\left[(\pi - 2\phi_0 + \sin 2\phi_0\cos 2\phi_0)(1-r^2) + 2r^2\sin^3 2\phi_0\right] - \mu\mu_0(1+\beta_0)\cos^4\phi_0\left(1+3r^2\sin^2\phi_0\right)\right\}$$

and $\frac{Q}{N\sqrt{3T}} = -\sqrt{\frac{2}{3\pi}}\left[(1-e) - \frac{2-eE}{2+eE}\frac{7}{2}\mu^2(1+e)\right]$, for all-sliding limit

where $\phi_0 = \arctan(\mu_0)$

Schneiderbauer et al.[30]

$$\frac{Q}{N\sqrt{3T}} = \frac{1}{\sqrt{6\pi}}\left\{2(e-1) + 3\mu^2(1+e) + \frac{\mu^2}{\mu_0^2}\exp\left(-\bar{u}^2\right)\cdot\left[6r^2(1+e-\mu_0) + 7(1+e) - 4\frac{\mu_0}{\mu}(1+\mu) - 3\mu_0^2(1+e)\right]\right\}$$

where $\bar{u} = \sqrt{\frac{3}{2}}\frac{r}{\mu_0}$

[a]The restriction on $r^2 \ge 1$ is always neglected in practice.

Schneiderbauer et al.'s model for different values of μ. When comparing Figures 6a with 5b, it is found that proper values for λ can further improve the predictions with Eq. 21. In addition, as observed in Figure 6a, a larger μ will cause more dissipation of fluctuation energy in the small sliding regime and more generation or thus less dissipation of fluctuation energy in the large sliding regime.

Figures 6b, c also show that the present model is quantitatively superior to Schneiderbauer et al.'s model under various values of β_0 and e. In Figure 6b, the increase of β_0 will cause more energy dissipation in the small sliding regime, but have no effects when the slip velocity is large enough. In Figure 6c, the decreasing of e will lead to more energy dissipation over the whole range of the slip velocity, and this trend is consistent with Louge's data. However, for highly inelastic particles (e.g., $e = 0.7$ or 0.5), the present model with constant λ based on Jenkins and Zhang's theory fails to predict the energy fluxes, especially in the small sliding regime. It is found that by increasing the values for λ, as inspired from Figures 4c, d, the predictions agree much better with Louge's data.

Rewriting the BCs

Following Johnson and Jackson,[27] BCs can be obtained by considering an infinitesimal volume in the granular flow in the shape of a pillbox with one face fixed on the wall. As the faces of the pillbox approach each other, the stress and energy flux at the wall should balance to those derived for the granular flow. Hence, the normal stress must satisfy

$$N = p_s \tag{22}$$

where p_s is the granular pressure. Then, the factor χ can be determined by this balance equation.

The BC for the mean granular velocity is obtained using the balance of the shear stress as

$$\mathbf{k}\cdot(\mu_s\nabla\mathbf{u})\cdot\mathbf{i} = -\mu\cot\Phi\sqrt{\frac{2}{\pi T}}\max(A_1,B_1)p_s(\mathbf{V}\cdot\mathbf{i}) \tag{23}$$

where μ_s is the granular shear stress. To calculate the slip velocity $\mathbf{V}$, the mean rotational velocity $\boldsymbol{\varpi}$ is needed. In the absence of solving its conservation equation, $\boldsymbol{\varpi}$ is often ignored or assumed equal to the angular velocity (half the vorticity) of the mean translational flow.[28,39] It is worthy to note that this BC only considers the instantaneous collisional stress, and for dense granular flow, additional quasistatic stress should be taken into account for particles in enduring contact.[31,41]

Similarly, the BC for the granular temperature is obtained as

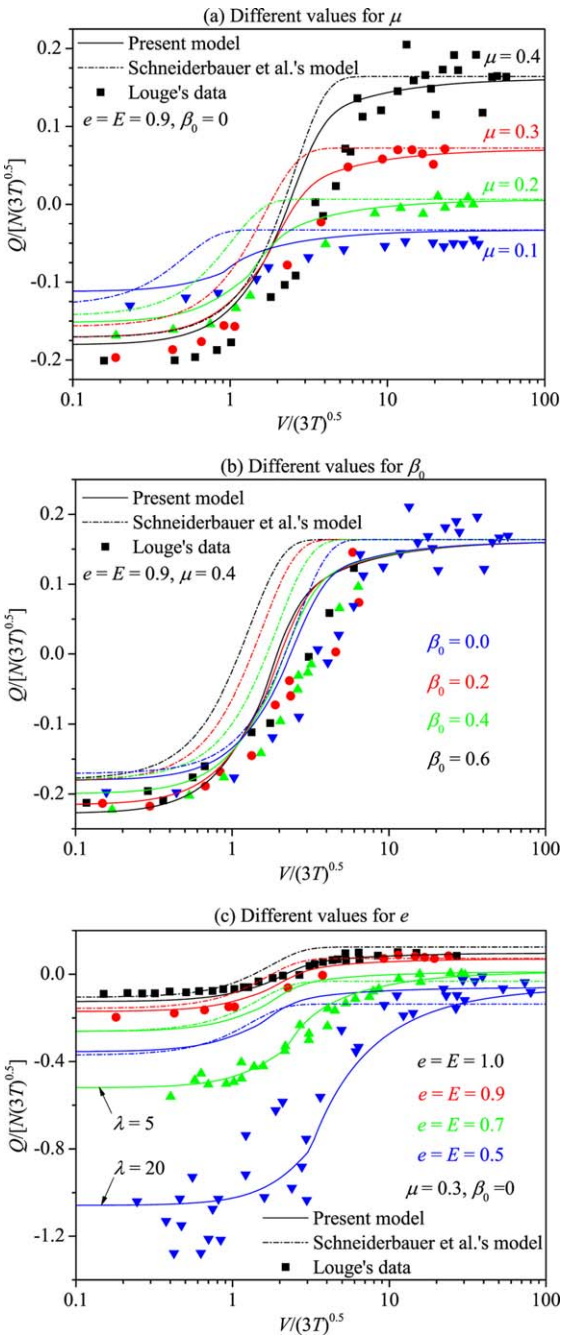

Figure 6. Normalized fluctuation energy fluxes over normalized slip velocity for different collisional parameters.

[Color figure can be viewed in the online issue, which is available at wileyonlinelibrary.com.]

$$\mathbf{k}\cdot(\kappa_s\nabla T) = -\sqrt{\frac{2T}{\pi}}\left\{\frac{2-eE}{2+eE}\frac{1+q}{q}\mu^2(1+e)\left[1-\frac{1}{X^2+1}\exp\left(-\frac{Y^2}{X^2+1}\right)\right] - (1-e)+(1+\lambda)\mu\cot\Phi\min(A_2,B_2)\right\}p_s \tag{24}$$

where κ_s is the granular energy diffusion coefficient. It should be noted that p_s, μ_s, and κ_s can be calculated according to the KTGF, whereas λ can be roughly calculated by the theory of Jenkins and Zhang[9] for a wide range of collisional parameters.

Conclusions

Using three collisional parameters for the particle-wall collisions and two granular temperatures for the particles' pseudothermal state, we propose general expression models

for the stresses and fluctuation energy fluxes of collisional granular flows at the flat wall. It is indicated by the granular temperature ratio λ that particle rotational velocity fluctuations have a great impact on both the shear stress and the energy flux. In fact, λ appears to be a Logistic function with respect to the normalized slip velocity. With proper and variable λ, new models would agree excellently with the particle simulations by Louge.[26] However, it is more practical and easier to obtain the constant λ through the theory of Jenkins and Zhang.[9] With the constant λ, new models still perform better than the previous models, and have adequate accuracy for cases of nearly elastic particles. While for highly inelastic particles, the performance of the new models can be improved by increasing the constant values of λ. In addition, the influence of different collisional parameters on the shear stress and energy flux are well represented by the new models. Nevertheless, further researches are still needed to theoretically clarify the correction on the flux of fluctuation energy and develop a model for λ to incorporate the effects of slip velocity as well as that of the collisional parameters.

Finally, on the above bases, new BCs are established for the velocity and granular temperature of collisional granular flows. They can now be reasonably used along with the effective coefficient approach within the framework of KTGF.

Acknowledgment

This work was supported by the National Science Foundation of China through Grant No. 51006089.

Notation

A_1, A_2, B_1, B_2 = dimensionless factors
$\mathbf{c}$ = translational velocity
$\mathbf{C}$ = fluctuating translational velocity
e = normal restitution coefficient for particle-wall collision
E = normal restitution coefficient for particle–particle collision
$\mathbf{G}$ = relative velocity of the point of contact
$\mathbf{i}$ = unit tangential vector
I = moment of rotary inertia
$\mathbf{J}$ = impulse
$\mathbf{k}$ = unit normal vector pointing into the flow
m = mass of particle
n = particle number density
N = normal stress
p_s = solid-phase pressure
$q = \frac{4I}{m\sigma^2}$, dimensionless moment of rotary inertia
Q = flux of fluctuation energy
S = shear stress
T = translational granular temperature
$\mathbf{u}$ = mean translational velocity
$\mathbf{v}$ = velocity of the moving wall
$\mathbf{V}$ = mean slip velocity
X, Y = dimensionless variables

Greek letters

β_0 = tangential restitution coefficient
χ = dimensionless correction factor to the particle distribution
ϕ = collision angle
Φ = critical collision angle
κ_s = energy diffusion coefficient of the solid phase
$\lambda = \frac{\Theta}{qT}$, granular temperature ratio
μ = friction coefficient
μ_s = solid-phase viscosity
Θ = rotational granular temperature
σ = particle diameter
$\boldsymbol{\varpi}$ = mean rotational velocity
$\boldsymbol{\omega}$ = rotational velocity
$\boldsymbol{\Omega}$ = fluctuating rotational velocity
ψ = particle property

Subscripts and superscripts

$'$ = postcollisional
i = i direction
ij = i-j plane
k = k direction
r = rotational
st = sticking
sl = sliding
t = translational

Literature Cited

1. Sundaresan S. Modeling the hydrodynamics of multiphase flow reactors: current status and challenges. *AIChE J*. 2000;46(6):1102–1105.
2. Lettieri P, Mazzei L. Challenges and issues on the CFD modeling of fluidized beds: a review. *J Comput Multiphase Flows*. 2009;1(2):83–131.
3. Jenkins JT, Richman MW. Grad's 13-moment system for a dense gas of inelastic spheres. *Arch Ration Mech Anal*. 1985;87(4):355–377.
4. Gidaspow D. *Multiphase Flow and Fluidization: Continuum and Kinetic Theory Description*. San Diego, CA: Academic Press, 1994.
5. Lun C, Savage S. A simple kinetic theory for granular flow of rough, inelastic, spherical particles. *J Appl Mech-T ASME*. 1987; 54(1):47–53.
6. Abu-Zaid S, Ahmadi G. Simple kinetic model for rapid granular flows including frictional losses. *J Eng Mech ASME*. 1990;116(2):379–389.
7. Lun C. Kinetic theory for granular flow of dense, slightly inelastic, slightly rough spheres. *J Fluid Mech*. 1991;233:539–559.
8. Goldshtein A, Shapiro M. Mechanics of collisional motion of granular materials. Part 1. General hydrodynamic equations. *J Fluid Mech*. 1995;282:75–114.
9. Jenkins JT, Zhang C. Kinetic theory for identical, frictional, nearly elastic spheres. *Phys Fluids*. 2002;14(3):1228–1235.
10. Kumaran V. The constitutive relation for the granular flow of rough particles, and its application to the flow down an inclined plane. *J Fluid Mech*. 2006;561:1–42.
11. Songprawat S, Gidaspow D. Multiphase flow with unequal granular temperatures. *Chem Eng Sci*. 2010;65(3):1134–1143.
12. Shuai W, Zhenhua H, Huilin L, Goudong L, Jiaxing W, Pengfei X. A bubbling fluidization model using kinetic theory of rough spheres. *AIChE J*. 2012;58(2):440–455.
13. Zhao YH, Lu B, Zhong YJ. Euler–Euler modeling of a gas–solid bubbling fluidized bed with kinetic theory of rough particles. *Chem Eng Sci*. 2013;104:767–779.
14. Goldschmidt M, Beetstra R, Kuipers JAM. Hydrodynamic modelling of dense gas-fluidised beds: comparison and validation of 3D discrete particle and continuum models. *Powder Technol*. 2004;142(1): 23–47.
15. Sun J, Battaglia F. Hydrodynamic modeling of particle rotation for segregation in bubbling gas-fluidized beds. *Chem Eng Sci*. 2006; 61(5):1470–1479.
16. Benyahia S. Verification and validation study of some polydisperse kinetic theories. *Chem Eng Sci*. 2006;63(23):5672–5680.
17. Shuyan W, Zhiheng S, Huilin L, Long Y, Wentie L, Yonlong D. Numerical predictions of flow behavior and cluster size of particles in riser with particle rotation model and cluster-based approach. *Chem Eng Sci*. 2008;63(16):4116–4125.
18. Yusuf R, Halvorsen B, Melaaen MC. An experimental and computational study of wall to bed heat transfer in a bubbling gas–solid fluidized bed. *Int J Multiphase Flow*. 2012;42:9–23.
19. Verma V, Deen NG, Padding JT, Kuipers J. Two-fluid modeling of three-dimensional cylindrical gas–solid fluidized beds using the kinetic theory of granular flow. *Chem Eng Sci*. 2013;102:227–245.
20. Benyahia S, Syamlal M, O'Brien TJ. Evaluation of boundary conditions used to model dilute, turbulent gas/solids flows in a pipe. *Powder Technol*. 2005;156(2):62–72.
21. Almuttahar A, Taghipour F. Computational fluid dynamics of high density circulating fluidized bed riser: study of modeling parameters. *Powder Technol*. 2008;185(1):11–23.
22. Li T, Grace J, Bi X. Study of wall boundary condition in numerical simulations of bubbling fluidized beds. *Powder Technol*. 2010; 203(3):447–457.
23. Lan X, Xu C, Gao J, Al-Dahhan M. Influence of solid-phase wall boundary condition on CFD simulation of spouted beds. *Chem Eng Sci*. 2012;69(1):419–430.
24. Chalermsinsuwan B, Chanchuey T, Buakhao W, Gidaspow D, Piumsomboon P. Computational fluid dynamics of circulating

fluidized bed downer: study of modeling parameters and system hydrodynamic characteristics. *Chem Eng J*. 2012;189:314–335.
25. Li T, Benyahia S. Evaluation of wall boundary condition parameters for gas–solids fluidized bed simulations. *AIChE J*. 2013;59(10): 3624–3632.
26. Louge MY. Computer-simulations of rapid granular flows of spheres interacting with a flat, frictional boundary. *Phys Fluids*. 1994;6(7): 2253–2269.
27. Johnson PC, Jackson R. Frictional–collisional constitutive relations for granular materials, with application to plane shearing. *J Fluid Mech*. 1987;176:67–93.
28. Jenkins JT. Boundary-conditions for rapid granular flow - flat, frictional walls. *J Appl Mech-T ASME*. 1992;59(1):120–127.
29. Jenkins JT, Louge MY. On the flux of fluctuation energy in a collisional grain flow at a flat, frictional wall. *Phys Fluids*. 1997;9(10): 2835–2840.
30. Schneiderbauer S, Schellander D, Loderer A, Pirker S. Non-steady state boundary conditions for collisional granular flows at flat frictional moving walls. *Int J Multiphase Flow*. 2012;43:149–156.
31. Schneiderbauer S, Aigner A, Pirker S. A comprehensive frictional-kinetic model for gas-particle flows: analysis of fluidized and moving bed regimes. *Chem Eng Sci*. 2012;80:279–292.
32. Walton OR. Numerical simulation of inelastic, frictional particle–particle interactions. In: Roco MC, editor. *Particulate Two-Phase Flow*. London: Butterworth-Heinemann, 1993:884–911.
33. Foerster SF, Louge MY, Chang H, Allia K. Measurements of the collision properties of small spheres. *Phys Fluids*. 1994;6:1108–1115.
34. Lorenz A, Tuozzolo C, Louge M. Measurements of impact properties of small, nearly spherical particles. *Exp Mech*. 1997;37(3):292–298.
35. Wu X, Wang Q, Luo Z, Fang M, Cen K. Experimental investigation of interparticle collision in the upper dilute zone of a cold CFB riser. *Int J Multiphase Flow*. 2008;34(10):924–930.
36. Sommerfeld M, Huber N. Experimental analysis and modelling of particle-wall collisions. *Int J Multiphase Flow*. 1999;25(6):1457–1489.
37. Gorham DA, Kharaz AH. The measurement of particle rebound characteristics. *Powder Technol*. 2000;112(3):193–202.
38. Kharaz AH, Gorham DA, Salman AD. An experimental study of the elastic rebound of spheres. *Powder Technol*. 2001;120(3):281–291.
39. Li TW, Benyahia S. Revisiting Johnson and Jackson boundary conditions for granular flows. *AIChE J*. 2012;58(7):2058–2068.
40. McCoy BJ, Sandler SI, Dahler JS. Transport properties of polyatomic fluids. IV. The kinetic theory of a dense gas of perfectly rough spheres. *J Chem Phys*. 1966;45(10):3845–3512.
41. Schneiderbauer S, Pirker S. Filtered and heterogeneity-based subgrid modifications for gas–solid drag and solid stresses in bubbling fluidized beds. *AIChE J*. 2013;60(3):839–854.

Appendix A

To do the calculation of the integral in Eq. 11, the error function is expanded into its Taylor series so that the integral can be written as

$$S_i = mn\chi \frac{\mu(1+e)}{4\pi(\lambda+1)} \frac{2}{\sqrt{\pi}} \sum_{\alpha=0}^{\infty} \frac{(-1)^{\alpha}(\cot\Phi)^{2\alpha+1}}{\alpha!(2\alpha+1)} \left(\frac{V_i}{\sqrt{2T}} I_\alpha + II_\alpha \right) \tag{A1}$$

where

$$I_\alpha = \int \left(\frac{G_{ij}}{\sqrt{2T}} \right)^{2\alpha} \exp\left[\frac{-|\mathbf{G}_{ij}-\mathbf{V}|^2}{2T(\lambda+1)} \right] d\mathbf{G}_{ij} \tag{A2}$$

$$II_\alpha = \int \frac{(G_i - V)_i}{\sqrt{2T}} \left(\frac{G_{ij}}{\sqrt{2T}} \right)^{2\alpha} \exp\left[\frac{-|\mathbf{G}_{ij}-\mathbf{V}|^2}{2T(\lambda+1)} \right] d\mathbf{G}_{ij} \tag{A3}$$

To simplify the notation we introduce the abbreviations $X = \sqrt{\lambda+1}\cot\Phi$ and $Y = \sqrt{V^2/2T}\cot\Phi$ into the following analysis. In situations when the ratio $\xi = Y/X$ is a small quantity, the integrals I_α and II_α are then carried out up to terms of order $O(\xi^2)$, and using the inductive method they can be, respectively, expressed as

$$I_\alpha = 2\pi T\left(1+\alpha\cdot\xi^2\right)\alpha!(\lambda+1)^{\alpha+1} \tag{A4}$$

$$II_\alpha = \frac{V_i}{\sqrt{2T}} 2\pi T\left[\alpha + \frac{\alpha}{2}(\alpha-1)\cdot\xi^2\right]\alpha!(\lambda+1)^{\alpha+1} \tag{A5}$$

Substituting Eqs. A4 and A5 into Eq. A1, the final expression can be obtained using the mathematical software Maple, thus we get

$$\frac{S_i}{N} = \mu\cot\Phi\sqrt{\frac{2}{\pi T}}V_i\left\{\frac{1}{2}\left(\frac{1}{X^2+1}+\frac{\arctan X}{X}\right)+\frac{\xi^2}{8}\left[\frac{1-X^2}{(1+X^2)^2}-\frac{\arctan X}{X}\right]\right\} \tag{A6}$$

Similarly, when $\xi^{-1} = X/Y$ is small, then the integrals I_α and II_α are carried out up to terms of order $O(\xi^{-2})$, and finally they can be expressed, respectively, as

$$I_\alpha = 2\pi T(\lambda+1)\left(1+\alpha^2\cdot\xi^{-2}\right)\left(\frac{V^2}{2T}\right)^{\alpha} \tag{A7}$$

$$II_\alpha = \frac{V_i}{\sqrt{2T}} 2\pi T(\lambda+1)\left(\alpha\cdot\xi^{-2}\right)\left(\frac{V^2}{2T}\right)^{\alpha} \tag{A8}$$

Using Eqs. A7 and A8 in Eq. A1, we can obtain

$$\frac{S_i}{N} = \mu\cot\Phi\sqrt{\frac{2}{\pi T}}V_i\left\{\frac{\sqrt{\pi}}{2}\frac{\mathrm{erf}(Y)}{Y}-\frac{\xi^{-2}}{4} \times\left[\frac{\sqrt{\pi}}{2}\frac{\mathrm{erf}(Y)}{Y}+\left(2Y^2-1\right)\exp\left(-Y^2\right)\right]\right. \tag{A9}$$

As shown in Figure A1, approximated analysis solutions using both Eqs. A6 and A9 are compared with the numerical integration for different values of λ. It is found that a combination of Eqs. A6 and A9 with a simple Max function can work

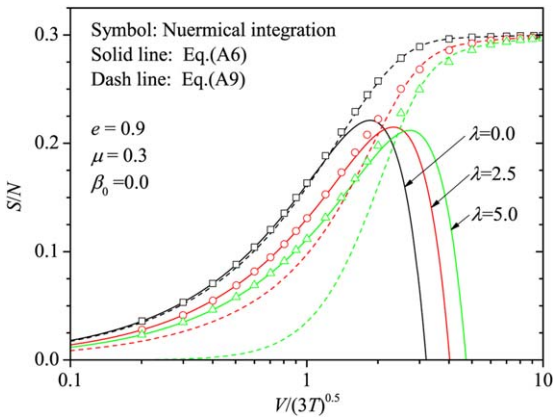

Figure A1. Comparison of the approximated analytical solution with numerical solution for the stress.

[Color figure can be viewed in the online issue, which is available at wileyonlinelibrary.com.]

well from nonsliding to all-sliding limits, and the junction looks very natural when λ is small.

Appendix B

The integral part in Eq. 15 can be written as

$$Q_{\mathrm{t}}^{III}=mn\chi\frac{\mu(1+e)}{4\pi(\lambda+1)^2}\int\frac{\mathbf{G}_{ij}\cdot\mathbf{G}_{ij}}{G_{ij}}\mathrm{erf}\left(\frac{G_{ij}\cot\Phi}{\sqrt{2T}}\right)\times\exp\left[\frac{-|\mathbf{G}_{ij}-\mathbf{V}|^2}{2T(\lambda+1)}\right]d\mathbf{G}_{ij}-\frac{\mathbf{S}\cdot\mathbf{V}}{(\lambda+1)} \tag{B1}$$

To calculate the integral, the Error function is expanded into its Taylor series and we have

$$Q_{\mathrm{t}}^{III}=mn\chi\frac{\mu(1+e)}{2\pi(\lambda+1)^2}\frac{\sqrt{2T}}{\sqrt{\pi}}\sum_{\alpha=0}^{\infty}\frac{(-1)^{\alpha}(\cot\Phi)^{2\alpha+1}}{\alpha!(2\alpha+1)}III_{\alpha}-\frac{\mathbf{S}\cdot\mathbf{V}}{(\lambda+1)} \tag{B2}$$

where

$$III_{\alpha}=\int\left(\frac{G_{ij}}{\sqrt{2T}}\right)^{2\alpha+2}\exp\left[\frac{-|\mathbf{G}_{ij}-\mathbf{V}|^2}{2T(\lambda+1)}\right]d\mathbf{G}_{ij}=I_{\alpha+1} \tag{B3}$$

If $\xi=Y/X$ is small, the second part in Eq. B2 can be calculated using Eq. A6 and is actually of order $O(\xi^4)$. Then, the integral III_{α} is carried out up to terms of order $O(\xi^4)$ and expressed inductively as

$$III_{\alpha}=2\pi T\left[1+(\alpha+1)\cdot\xi^2+\frac{\alpha}{4}(\alpha+1)\cdot\xi^4\right](\alpha+1)!(\lambda+1)^{\alpha+2} \tag{B4}$$

Employing Eqs. B4 and A6 into Eq. B2 and using the mathematical software Maple, we have

$$\frac{Q_{\mathrm{t}}^{III}}{N\sqrt{3T}}=\sqrt{\frac{2}{3\pi}}\mu\cot\Phi\left\{\left(\frac{1}{X^2+1}+\frac{\arctan X}{X}\right)-\frac{\xi^2}{2}\left[\frac{X^2-1}{(X^2+1)^2}+\frac{\arctan X}{X}\right]+\frac{3\xi^4}{16}\left[\frac{(3X^2+1)(X^2-3)}{3(X^2+1)^3}+\frac{\arctan X}{X}\right]\right\} \tag{B5}$$

If $\xi^{-1}=X/Y$ is small, the integral III_{α} is carried out up to terms of order $O(\xi^{-4})$ and expressed inductively as

$$III_{\alpha}=2\pi T(\lambda+1)\left[1+(\alpha+1)^2\cdot\xi^{-2}+\frac{\alpha^2}{2}(\alpha+1)^2\cdot\xi^{-4}\right]\left(\frac{V^2}{2T}\right)^{\alpha+1} \tag{B6}$$

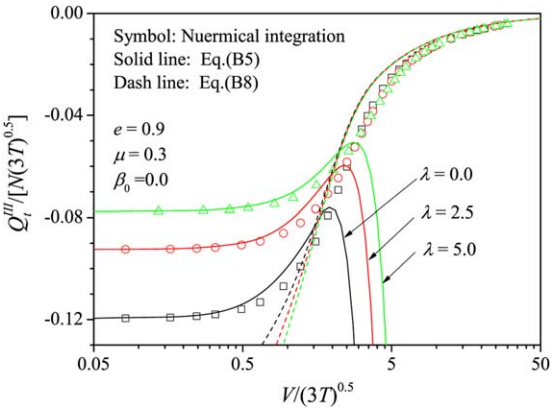

Figure B1. Comparison of the approximated analytical solution with numerical solution for the energy flux term.

[Color figure can be viewed in the online issue, which is available at wileyonlinelibrary.com.]

Using Eqs. B6 and A9 into Eq. B2, we obtain

$$\frac{Q_{\mathrm{t}}^{III}}{N\sqrt{3T}}=\sqrt{\frac{2}{3\pi}}\mu\cot\Phi\left\{\frac{\sqrt{\pi}}{2}\frac{\mathrm{erf}(Y)}{Y}+\exp\left(-Y^2\right)+\frac{\xi^{-2}}{16}\left[\frac{\sqrt{\pi}}{2}\frac{\mathrm{erf}(Y)}{Y}-\left(8Y^6-36Y^4+22Y^2+1\right)\exp\left(-Y^2\right)\right]\right\} \tag{B7}$$

In the square bracket of Eq. B7, the first term is found to be dominant when Y is of large magnitude (e.g., $|Y|>4$), whereas the second term can cause a numerical oscillation when Y is of small magnitude. Thus, to guarantee a numerical stability, the second term is dropped, and we have

$$\frac{Q_{\mathrm{t}}^{III}}{N\sqrt{3T}}=\sqrt{\frac{2}{3\pi}}\mu\cot\Phi\left[\left(1+\frac{\xi^{-2}}{16}\right)\frac{\sqrt{\pi}}{2}\frac{\mathrm{erf}(Y)}{Y}+\exp\left(-Y^2\right)\right] \tag{B8}$$

Figure B1 compares the approximated analysis solutions using Eqs. B5 and B8 with the numerical integration for different values of λ. As observed, Eq. B5 is excellent in the small sliding regime and Eq. B8 is excellent in the large sliding regime, but they both may underestimate the flux magnitude in the transition regime. However, a combination of Eqs. B5 and B8 with a simple Min function (excluding the minus cotΦ) can still be recommended.

Manuscript received Apr. 29, 2014, and revision received July 14, 2014.